DEUTSCHES ELEKTRONEN-SYNCHROTRON DESY

DESY 90-133
November 1990

Recent Crystal Ball Results on Resonance Formation in $\gamma\gamma$-Reactions

J. K. Bienlein

Deutsches Elektronen-Synchrotron DESY, Hamburg

ISSN 0418-9833

NOTKESTRASSE 85 · 2 HAMBURG 52

To be sure that your preprints are promptly included in the HIGH ENERGY PHYSICS INDEX , send them to the following address (if possible by air mail) :

DESY
Bibliothek
Notkestrasse 85
2 Hamburg 52
Germany

DESY 90-133
November 1990

ISSN 0418-9833

RECENT CRYSTAL BALL RESULTS ON RESONANCE FORMATION IN $\gamma\gamma$–REACTIONS *

J.K. BIENLEIN

Deutsches Elektronen-Synchrotron, Notkestrasse 85, D-2000 Hamburg 52, Germany
Representing the Crystal Ball Collaboration

The Crystal Ball detector has been used for $\gamma\gamma$–production of final states consisting of π^0's and η's only. New results are obtained for $\gamma\gamma \to \pi^0\pi^0\pi^0$ where the $\pi_2(1670)$ with $\Gamma_{\gamma\gamma}(\pi_2) = (1.41 \pm 0.23 \pm 0.28)$ keV has been observed. In $\gamma\gamma \to \eta\,\pi^0\pi^0$ a hitherto unknown resonance X (1900) was found with $\Gamma_{\gamma\gamma}(X)BR(X \to \eta\pi^0\pi^0) = (0.9 \pm 0.3 \pm 0.5)$ keV. The assignment is probably $J^{PC} = 2^{-+}$ suggesting $X = \eta_2$. The 2^{-+} mesons seem to be $q\bar{q}$ states. All data on $\gamma\gamma$–formation of resonances are summarized and used to get information on the charged constituents (quarks) of the hadrons and on possible gluon constituents by comparing to radiative J/ψ–decays.

1. INTRODUCTION

The process which is called a "$\gamma\gamma$–reaction" is shown in Fig. 1. Electrons and positrons in an e^+e^-–collider emit virtual photons γ^*. These can react to produce lepton pairs or hadrons. The Crystal Ball experiment whose results [1–7] will be presented here did not observe the scattered electrons $e^{-'}$ and positrons $e^{+'}$ ("no-tag mode") because most of them do not change their direction and disappear therefore in the beampipe. The virtual photons then have $q^2 \approx 0$ and are "quasi-real". The Crystal Ball data are also restricted to observe the formation of hadron resonances R which then decay into π^0's and η's. Resonance formation in $\gamma\gamma$–reactions implies that the quantum numbers of R have to be allowed for the $\gamma\gamma$–system: charge conjugation $C = +1$ and spin $J \neq 1$.

Experimental data (for reviews see [8–11]) exist now for many resonances (see table 1). So $\gamma\gamma$–physics has reached a certain maturity and it is time to ask the question: What can $\gamma\gamma$–formation of hadrons contribute to hadron spectroscopy? The main contribution will not be to observe new resonances (though this will also be reported here) but the measurement of hadron constituents. As photons couple to electric charges the underlying process to Fig. 1 is the coupling to the charged constituents (quarks) of hadrons (Fig. 2). So the $\gamma\gamma$ partial width of a resonance R will be proportional to the square of the mean squared-charge:

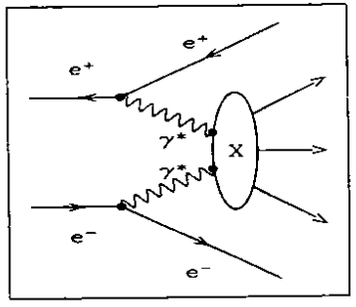

Figure 1: The diagram for formation of a resonance X in $\gamma\gamma$ collisions, X decaying into hadrons.

$$\Gamma_{\gamma\gamma}(R) \sim \langle c_R^2 \rangle^2.$$

New results for hadron spectroscopy which develops to hadron microscopy can be gained by combining $\Gamma_{\gamma\gamma}(R)$ with other information:

1. The quark composition ($u\bar{u}$, $d\bar{d}$, and/or $s\bar{s}$) of isoscalar mesons in $q\bar{q}$ nonets ("singlet-octet mixing") by comparing the $\gamma\gamma$ partial widths of the three I_3=0 members of the nonet.

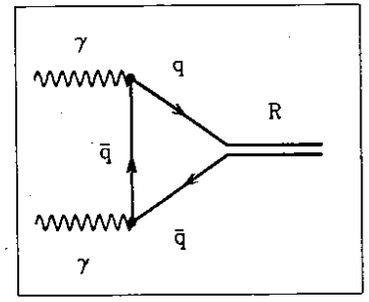

Figure 2: The $\gamma\gamma$–coupling to a meson with quark constituents.

2. Gluon constituents in $q\bar{q}$ mesons and in glueballs can be identified by comparing (g=gluon) $\gamma\gamma \to R$ with $gg \to R$ (from the radiative J/ψ decay $J/\psi \to \gamma gg \to \gamma R$).

3. Multiquark states are more difficult to identify. One can use the size of $\Gamma_{\gamma\gamma}(R)$, especially by comparing various resonances to each other and to theoretical models.

Some general remarks on $\gamma\gamma$–experiments should be made:

1. $\gamma\gamma$–experiments are wide-band beam reactions, i.e. both photons have a continuous energy spectrum.

2. The event rate is low. The number of seen events N is given by

$$N = L_{ee} \int (d\Phi_{\gamma\gamma}/dW_{\gamma\gamma})\, dW_{\gamma\gamma} \cdot \sigma(\gamma\gamma \to R) \cdot BR(R \to \text{f.s.}) \cdot \epsilon$$

($L_{ee} = e^+e^-$ luminosity, $W_{\gamma\gamma} = \gamma\gamma$ center-of-mass energy, $\Phi_{\gamma\gamma}(W_{\gamma\gamma}) = \gamma\gamma$–flux, σ = cross section, BR = branching ratio, f.s. = observed final state, ϵ = detection efficiency).

A comparison of rates for $\gamma\gamma$–reactions with e^+e^- annihilation shows (numbers for the Crystal Ball experiment):

a. $\gamma\gamma$–flux:

$$L_{\gamma\gamma} = L_{ee} \int_{1\text{GeV}}^{5\text{GeV}} (d\Phi_{\gamma\gamma}/dW_{\gamma\gamma})\, dW_{\gamma\gamma} \approx 10^{-2} L_{ee}.$$

b. cross sections
$\sigma(\gamma\gamma \to f_2(1270) \to \pi^0\pi^0) = 170$ nb,
$\sigma_{tot}(e^+e^- \to h$ at 10 GeV$) = 2.9$ nb, i.e.
$\sigma(\gamma\gamma) \approx 60 \times \sigma(e^+e^-)$

c. $\epsilon_{\gamma\gamma} \approx 3\%$ because of the Lorentz-boost of the $\gamma\gamma$ center-of-mass system in the laboratory frame (a consequence of having a wide-band beam), but $\epsilon_{e^+e^-} \approx 100$ %.

Combining the numbers one finds that the number of $\gamma\gamma$–produced f_2–mesons is about a factor 60 smaller than the number of continuum events.

For $\gamma\gamma$–experiments not only event rates are low, also the analysis is more complicated. As a consequence $\gamma\gamma$–experiments take a longer time to get out results.

2. CRYSTAL BALL PERFORMANCE FOR $\gamma\gamma$–PHYSICS

2.1. The Crystal Ball detector (= CB)

The Crystal Ball detector (Fig. 3) is a calorimeter for electromagnetically showering particles (electrons and photons) [3,14,15]. It was designed to have the best possible energy resolution. The main ball consists of 672 NaI(Tl) crystals of 16 radiation lengths which cover 93% of 4π sr solid angle. The beampipe is surrounded by four double-layers of proportional tubes which are used here to veto charged particles. The solid angle up to 98% is covered by 40 NaI(Tl) endcap crystals which will be used also for vetos.

The Crystal Ball detector was operated at the DORIS-II e^+e^- storage ring around 10 GeV center-of-mass energies in the years 1982 to 1986. An integrated luminosity of $L_{ee} \sim 250$ pb^{-1} was collected.

*Talk presented at the QCD90 Workshop, July 8-13, 1990 at Montpellier (France)

Table 1: List of observed and unobserved states in $\gamma\gamma$–formation. Quantum numbers and quark model assignments are also shown. The decay modes seen by CB are given. The $f_2'(1525)$ is not accessible by CB.

Measured mesons					
Meson multiplet		$I=1$	$I=0$	$I=0$	$I=0$
J^{PC}	quark model assignment				
0^{-+}	$^1S_0$	π^0 $\rightarrow \gamma\gamma$	η $\rightarrow \gamma\gamma$ $\rightarrow \pi^\circ\pi^\circ\pi^\circ$	η' $\rightarrow \gamma\gamma$ $\rightarrow \eta\pi^\circ\pi^\circ$	η_c $\rightarrow \eta\pi^\circ\pi^\circ$ (1 event)
0^{++}	$^3P_0$	$a_0(980)$ $\rightarrow \eta\pi^\circ$	$f_0(975)$ $\rightarrow \pi^\circ\pi^\circ$ limit		
2^{++}	$^3P_2$	$a_2(1320)$ $\rightarrow \eta\pi^\circ$	$f_2(1270)$ $\rightarrow \pi^\circ\pi^\circ$	$f_2'(1525)$ $K\bar{K}$	
2^{-+}	$^1D_2$	$\pi_2(1670)$ $\rightarrow \pi^\circ\pi^\circ\pi^\circ$	$\eta_2(1876)$? $\rightarrow \eta\pi^\circ\pi^\circ$		
Production of threshold continua					
$\gamma\gamma \rightarrow \pi^\circ\pi^\circ$					
$\gamma\gamma \rightarrow \pi^\circ\eta$					
Limits on unobserved, but expected states					
radial excitations of π°		$\pi^\circ(1300)$ etc.			
radial excitations of η		$\eta(1275)$ etc.			
gluonium candidates		$\eta(1440), f_0(1590), f_2(1720), f_2(2220)$			

2.2. Standard performance

a. Photons deposit energy in 13 neighbouring crystals (Fig. 5a). The energy calibration is linear with pulseheight, small corrections are applied for longitudinal and transversal shower leakage ($\sim 2\%$), for non-central hits in the bump crystal ($\sim 2\%$) and for a small non-linearity at lower photon energies ($\sim 5\%$ at 100 MeV). The energy resolution is

$$\frac{\sigma_E}{E} = \frac{(2.7 \pm 0.2)\%}{\sqrt[4]{E/GeV}} \quad (= 5\% \text{ at } 100\ MeV),$$

the angular resolution

$\sigma_\theta = 1^\circ$ for high E_γ
(using the lateral shower distribution)

$\sigma_\theta = 3^\circ$ for low E_γ
(given by the crystal granularity)

$\sigma_\phi = \sigma_\theta / \sin\theta$.

Photon identification is done by requiring

1. no charged track in the tube chambers correlated with the energy deposition in the calorimeter, and

2. a lateral shower distribution which is consistent with an electromagnetic shower, thus rejecting minimum ionizing hadrons and muons as well as interacting hadrons and overlapping γ–showers. As the efficiency of these cuts is around 50% per γ it was important to develop selection methods which can avoid them.

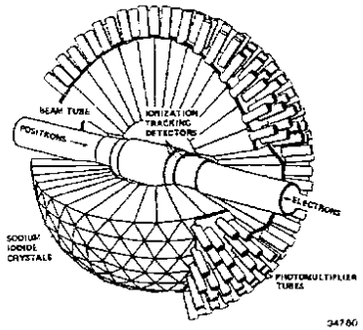

Figure 3: Crystal Ball detector (artist's view) showing the main ball NaI(Tl)–crystals with photomultipliers and tube chamber layers around the beampipe.

b. π°- and η–mesons are measured by their decay mode into $\gamma\gamma$. Fig. 4 shows e.g. the $\gamma\gamma$ invariant mass distributions for events which contain six photons.

One obtains the mass resolutions of 10 MeV at $m(\pi^\circ)$, 20 MeV at $m(\eta)$ and of 50 MeV at 2 GeV.

The two photons start to overlap and to merge into one shower for higher π^0 energies. This is due to the fact that the minimum opening angle (which is the most possible case) between the two photons from π° decay depends on the π° energy E_{π° by $\sin\theta_{min} = m_{\pi^\circ}/E_{\pi^\circ}$. Given the granularity of the CB detector the probability for overlap is 10 % at 600 MeV and 90 % at 1100 MeV.

Fig. 5 shows the lateral shower distribution of a single photon which contains one local maximum (the bump crystal) and of a π° with two local maxima. This observation is used in a quantitative way by calculating the second moment S of the shower distribution. Adjacent crystals with $E_{\text{crystal}} > 10$ MeV are called a connected region (CR). We calculate the

π° energy $\quad E_{\pi^\circ} = \sum_{CR} E_i$

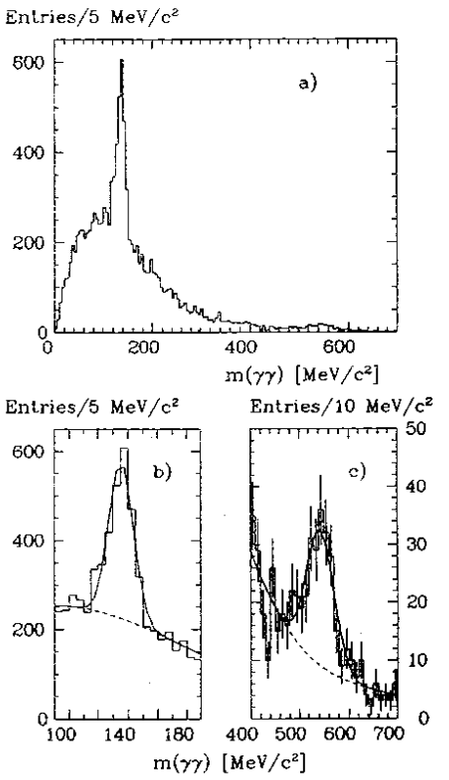

Figure 4: The $\gamma\gamma$ invariant mass for six photon final states. The π^0– and η–mesons are seen. a) Overall plot (15 entries/event), b), and c) the mass resolutions of the π^0 and η, respectively.

π° direction $\quad \vec{c} = (1/E_{\pi^\circ}) \sum_{CR} E_i \vec{n_i}$
($\vec{n_i}$ = unit vector to crystal i)

$S = (1/E_{\pi^\circ}) \sum_{CR} E_i (\vec{n_i} - \vec{c})^2$

π° mass $\quad m_{\pi^\circ} = E_{\pi^\circ}\sqrt{S - S_\gamma}$ (S_γ = 2nd moment of γ's)

Examples will be given below.

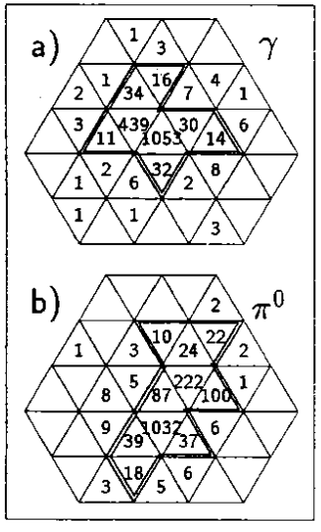

Figure 5: The lateral distribution of showers in the Crystal Ball, a) single photon with one local maximum (bump), b) two photons from π°−decay with two local maxima.

2.3. Special CB features for $\gamma\gamma$−physics

Some features of the Crystal Ball detector render it well suited for $\gamma\gamma$−physics.

1. CB can operate with low trigger thresholds E_{tr}. It is
   E_{tr} = 8% $E_{c.m.}$ with standard $\gamma\gamma$ trigger
   = 0.8% $E_{c.m.}$ with dedicated $\gamma\gamma$ trigger
   To avoid unacceptable high trigger rates one imposes in addition the transverse balance of the energy deposition and eventually no charged spray.

2. CB has a large solid angle to compete with the effects of the Lorentz-boost of the $\gamma\gamma$−system. The coverage is 93%×4π sr for the main ball NaI crystals of which 85%×4π sr have full shower containment and up to 98%×4π sr can be used for vetoes. As important is the low E_γ threshold in the crystals (E_{th} = 10 MeV, = 20 MeV in earlier work) because of the asymmetric π° decays.

3. The "all-neutral final state" which is accessible for CB acts as a "filter". E.g. no resonance decay via ρ° can be observed. The remaining allowed channels have less background. This turned out to be a favourable feature.

2.4. Limitations of the CB detector

Limitations of the CB detector have shown to be less important for $\gamma\gamma$−physics. As the CB does not have an energy measurement of charged particles it can fully reconstruct only all-neutral final states. This turns into an advantage for the accessible reactions. The granularity of the CB is determined by the lateral shower width which in turn is given by the NaI radiation length. A shower occupies 13 crystals, with a guard ring they are 37 crystals. So an event with 10 photons occupies more than 50% of the crystals (if equally spaced). Overlaps reduce the efficiency. But the resonances which are produced in $\gamma\gamma$−reactions have low multiplicities in their decay. So this limitation is unimportant for $\gamma\gamma$−reactions.

3. RECENT RESULTS

Recent results of the Crystal Ball collaboration concern the channels

$$\gamma\gamma \rightarrow \left\{ \begin{array}{ccc} \pi^\circ & \pi^\circ & \pi^\circ \\ \eta & \pi^\circ & \pi^\circ \end{array} \right\} \rightarrow 6\,\gamma$$

In these channels the $\pi_2(1670)$ meson and a hitherto unknown (but expected) resonance, possibly the isoscalar partner $\eta_2(1875)$, are observed.

3.1. $\gamma\gamma \rightarrow \pi^\circ\pi^\circ\pi^\circ \rightarrow 6\,\gamma$

This channel is identified by reconstructing three π°'s out of six photons [5]. At low center-of-mass energies $W_{\gamma\gamma}$ (= $M(3\pi^\circ)$, the invariant mass of the $3\pi^\circ$ system which is measured) the η−meson is seen − and nothing else. For higher invariant masses ($M(3\pi^\circ) \geq$ 1 GeV/c^2) the π°'s are more energetic and the two photons from at least one π°overlap and merge into one energy cluster. So the selection criteria are:
1 "merged π°" with $E_{CR} > 500$ MeV

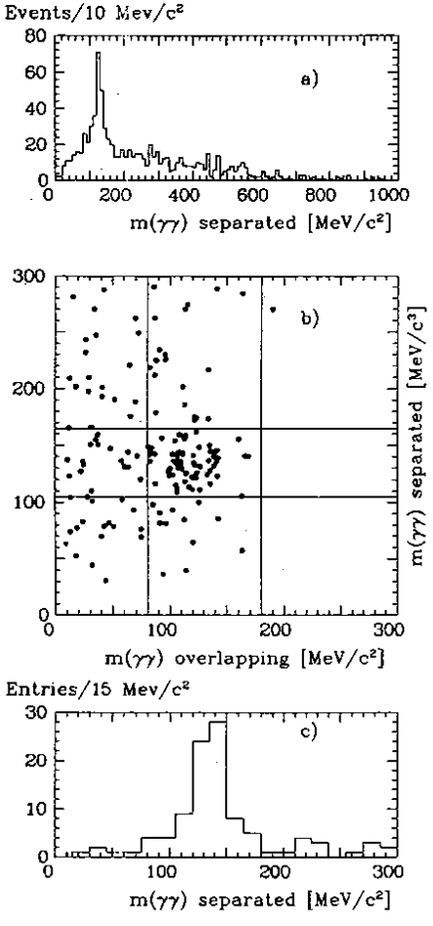

Figure 6: Selection of the $\pi^\circ\pi^\circ\pi^\circ$ state. a) $\gamma\gamma$ against invariant mass of the four photons (three entries/event). The π° is seen. b) Scatter plot of the invariant mass of one of the unmerged π°'s against the invariant mass of the overlapping shower candidate (from the second moment of the shower distribution). The cut window is displayed. c) $\gamma\gamma$ invariant mass distribution of the remaining pair from plot b).

4 separated γ−showers
$\leq 1\,\gamma$ is allowed to convert in the beampipe or the track detector
$|\sum p_T| < 100$ MeV/c to assure $\gamma\gamma$ origin and exclusive observation of the $3\pi^\circ$ final state.

The selection sequence is seen in Fig. 6. The $\gamma\gamma$ invariant mass distribution of the four separated γ−showers shows a clear π° peak (Fig. 6a). The scatter plot of the invariant mass of one pair of photons against the invariant mass of the two overlapping photons (Fig. 6b) shows that the data sample contains events with two π°'s. We now cut out those events and plot for them the invariant mass of the remaining $\gamma\gamma$−pair (Fig. 6c). As a result we observe a $\pi^\circ\pi^\circ\pi^\circ$ final state with low background.

For this data sample of 69 events we plot the event spectrum in Fig. 7. Above a small background we find a peak. We first prove that it is not an artefact produced by a trigger and acceptance threshold at low invariant masses $M(\pi^\circ\pi^\circ\pi^\circ)$ and the decreasing $\gamma\gamma$−flux on the high side. The expectation from the assumption of producing the $\pi^\circ\pi^\circ\pi^\circ$ state with a constant cross section and with phase space decay is also shown. It disagrees with the observation.

Next we show that the observed events really originate from $\gamma\gamma$−production of $\pi^\circ\pi^\circ\pi^\circ$. Fig. 8 shows the p_T^2−distributions. For $\gamma\gamma$−events it should be peaked at zero. This behaviour is found for the events with $M(\pi^\circ\pi^\circ\pi^\circ) \geq 1450$ MeV/c^2 (Fig.8b).
On the other hand events with
$M(\pi^\circ\pi^\circ\pi^\circ) < 1450$ MeV/c^2
show a flat p_T^2−distribution and are not $\gamma\gamma$−events (Fig. 8a)

Around 1700 MeV/c^2 a resonance is known [16] which is a candidate for the peak seen in this experiment. It is the $\pi_2(1670)$, a $J^{PC} = 2^{-+}$−state. It has been produced e.g. by $\pi^- p \rightarrow \pi_2^- p \rightarrow \pi^-\pi^+\pi^- p$. Four intermediate states are reported: $\pi_2 \rightarrow f_2\pi$ (BR = 56%).→ $\rho\pi$ (BR = 31%), → $(\pi\pi)_{S-wave}\pi$ (BR = 9% with 1.8 standard deviations), and → K^+K^- (BR

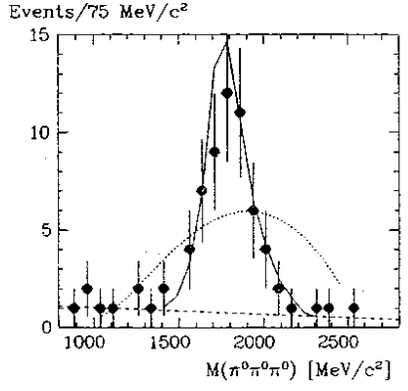

Figure 7: The raw event spectrum of $\pi^\circ\pi^\circ\pi^\circ$ final states with one merged π°. Also shown is the prediction for constant cross section and phase space decay (···) The background (- - -) and the Breit-Wigner fit(—) are described below. Data are the points.

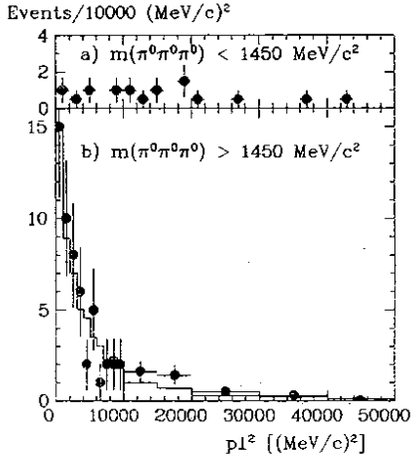

Figure 8: The $|\sum P_T^2|$-distribution of $\pi^\circ\pi^\circ\pi^\circ$ events (with one merged π°). a) for events with $M(\pi^\circ\pi^\circ\pi^\circ) \leq 1450$ MeV/c^2, b) for events with $M(\pi^\circ\pi^\circ\pi^\circ) > 1450$ MeV/c^2. Data: dots with error bars. Histogram: MC prediction for π_2 formation and decay.

$= 4\%$).

To confirm π_2°−production in the channel

$$\gamma\gamma \to \pi_2^\circ \to \pi^\circ\pi^\circ\pi^\circ \qquad (3.1)$$

we study the invariant mass distribution of the $\pi^\circ\pi^\circ$−subsystem. In Fig. 9 we see a clear $f_2 \to \pi^\circ\pi^\circ$ peak. It agrees with the Monte Carlo expectation from reaction chain (3.1) and disagrees with phase space decay. Next we measure the decay angular distributions (Fig. 10) of the "fast π°" (= most energetic π°), the two remaining π°'s and the normal of the decay plane, always with respect to the beam direction. The data are compared to expectations (Monte Carlo calculations) of a $J^P = 2^-$ decay with helicity 0, i.e. forward peaked angular distribution $\sim |Y_{2,0}|^2 \times$ detection efficiency, and an isotropic decay according to phase space. All three angular distributions agree with $J^P = 2^-$ and disagree with isotropy.

The calculations of the detection efficiency starts with the $\gamma\gamma$−generator. Calculating the matrix element for eq. (3.1) one has to realize that a $J^P = 2^-$ state can be formed from quasi-real photons only with helicity $\lambda = 0$. The $\pi_2 \to f_2\pi^\circ$ has the orbital angular momentum $L = 0$ so that the f_2 has the spin direction along the beam axis and its decay angular distribution is $\sim |Y_{2,0}(\Theta)|^2$ (Y = spherical harmonics) which is peaked forward. This, together with the Lorentz-boost from the asymmetric "γ−beam" energies, lowers the acceptance, compared to phase space decay, to $\epsilon \sim 1\%$. The photons are tracked in the detector. The efficiency at small values of $M(\pi^\circ\pi^\circ\pi^\circ)$ is mainly determined by the merged π°'s.

Now we can calculate the cross section, more precisely $\sigma(\gamma\gamma \to \pi_2)\, BR(\pi_2 \to \pi^\circ\pi^\circ\pi^\circ)$ according to the expression

$$\frac{dN}{dW_{\gamma\gamma}} = L_{ee}\, \frac{d\Phi_{\gamma\gamma}}{dW_{\gamma\gamma}}\, \sigma_{\gamma\gamma}\, \epsilon + \frac{dN}{dW_{\gamma\gamma}}|_{background}$$

It is shown in Fig. 11 together with the fit to a $J^{PC} = 2^{-+}$ Breit-Wigner resonance. The fit results are

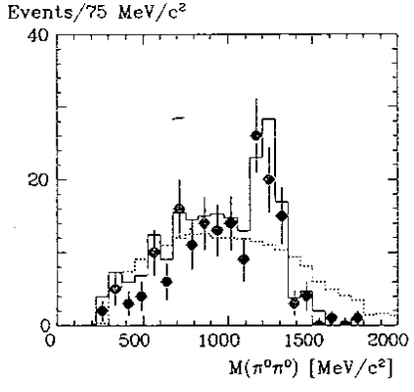

Figure 9: The invariant mass distribution of the $\pi^\circ\pi^\circ$−subsystem (3 entries/event) for events with $M(\pi^\circ\pi^\circ\pi^\circ) > 1450$ MeV/c^2. Data: dots with error bars. MC for π_2 production and decay: solid histogram. MC for production with constant cross section and phase space decay (dotted histogram).

$$M(\pi_2) = (1742 \pm 31 \pm 49)\ \text{MeV/c}^2$$
$$\Gamma_{tot}(\pi_2) = (236 \pm 49 \pm 36)\ \text{MeV/c}^2$$
$$\Gamma_{\gamma\gamma}(\pi_2) \times BR(\pi_2 \to \pi^\circ\pi^\circ\pi^\circ) = (251 \pm 40 \pm 35)\ \text{eV}$$
$$\Gamma_{\gamma\gamma}(\pi_2) = (1.41 \pm 0.23 \pm 0.28)\ \text{keV}$$

The main contributions to the systematic errors are

for M: energy calibration,

for Γ_{tot}: background subtraction,

for $\Gamma_{\gamma\gamma} \times BR$: detection efficiency, background subtraction, luminosity,

for $\Gamma_{\gamma\gamma}$: in addition π_2 decay branching ratios.

The CELLO collaboration has observed the π_2^0 (1670) in $\gamma\gamma$−production [12] by the reaction chain

$$\gamma\gamma \to \pi_2 \left\{ \begin{array}{l} \to f_2\pi^\circ \\ \to \rho^\pm\pi^\mp \end{array} \right\} \to \pi^+\pi^-\pi^\circ \qquad (3.2)$$

The analysis for the $\pi^+\pi^-\pi^0$ final state is more difficult as the dominant process is

$$\gamma\gamma \to a_2(1320) \to \rho^\pm\pi^\mp \to \pi^+\pi^-\pi^0. \qquad (3.3)$$

Fig. 12 gives the $M(\pi^+\pi^-\pi^0)$ distribution for the cases where the two photons from the π°−decay are observed

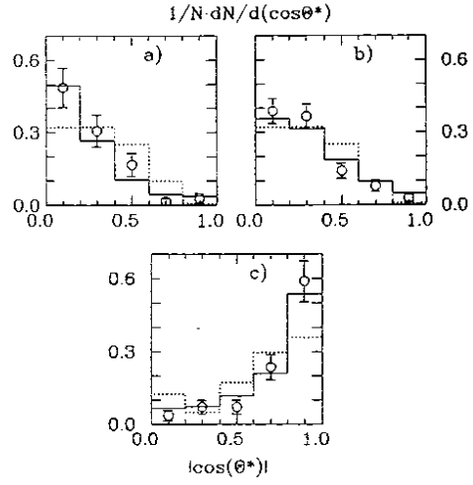

Figure 10: The angular distribution of $\pi^\circ\pi^\circ\pi^\circ$ events (always in the $\gamma\gamma$ center-of-mass system). a)θ^* (fast π°, beam), b)θ^* (remaining π°'s, beam), c)θ^* (normal to decay plane, beam). Data: circles with error bars. MC for π_2: solid line. MC with phase space decay: dotted line.

or only one. The invariant mass distribution of the $(\pi^+\pi^-)$−subsystem in the π_2 mass region (Fig. 13) shows the f_2 (1270) from π_2−decay. The result of the fit to these data depends on the relative phase of the various amplitudes. The CELLO collaboration obtains

$$M(\pi_2) = (1684 \pm 82)\ \text{MeV/c}^2$$

$$\Gamma_{tot}(\pi_2) = (540 \pm 320)\ \text{MeV}$$

$$\Gamma_{\gamma\gamma}(\pi_2) = (0.8 \pm 0.3 \pm 0.12)\ \text{keV}$$

assuming constructive interference and

$$\Gamma_{\gamma\gamma}(\pi_2) = 0.8 \text{ to } 1.5\ \text{keV}$$

depending on the interference.

Thus the $\gamma\gamma$−formation of the π_2 has been seen in two different final states.

3.2. $\gamma\gamma \to \eta\pi^\circ\pi^\circ \to 6\,\gamma$

The Crystal Ball collaboration has recently [6] used their full data sample of ~ 250 pb^{-1} and applied a data

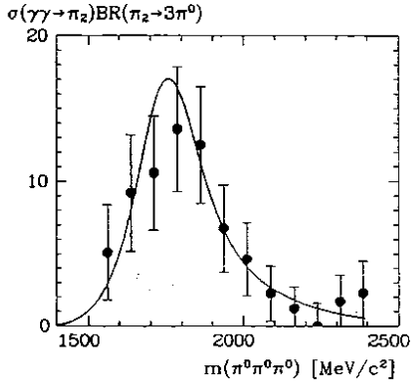

Figure 11: The cross section $\sigma(\gamma\gamma \to \pi_2)$ $\times BR(\pi_2 \to \pi^\circ\pi^\circ\pi^\circ)$ after all corrections. Data: dots with error bars. Fit to Breit-Wigner resonance with $J^P = 2^-$: full line.

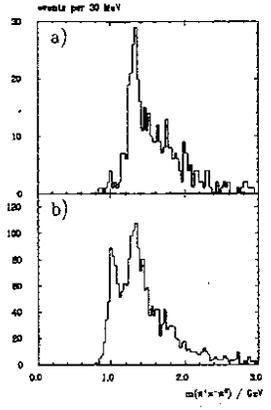

Figure 12: The invariant mass $M(\pi^+\pi^-\pi^\circ)$ as seen by CELLO, a) for events where both γ's from π° decay are detected, b) for events with only one γ. Plot b) shows also $\eta' \to \gamma\rho^0$, besides the $a_2(1320)$ and the tail containing the π_2.

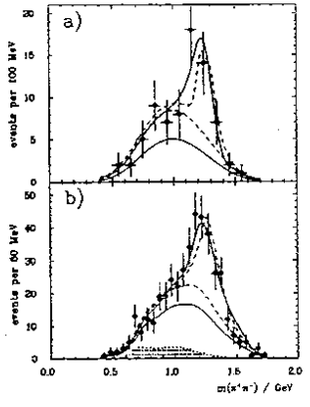

Figure 13: The invariant mass of the $\pi^+\pi^-$–subsystem in the π_2 mass range (CELLO data). a) for "two–γ events", b) for "one–γ events". Data: points with error bars. MC with constructive interference (solid line) and destructive interference (dashed line).

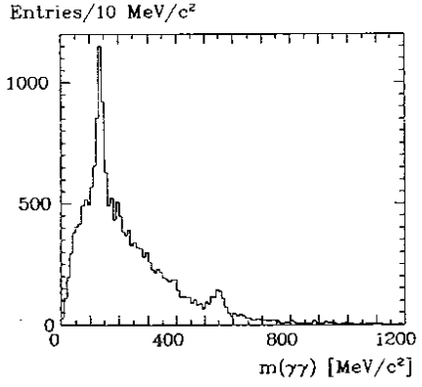

Figure 14: The $\gamma\gamma$ invariant mass distribution for events with six showers (15 entries/event.)

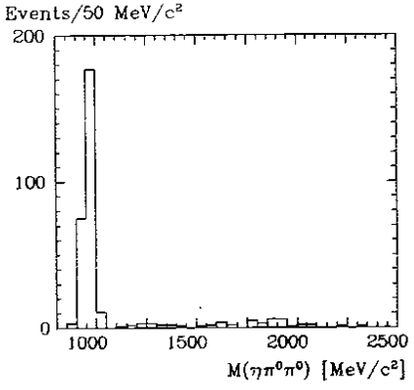

Figure 15: The invariant mass spectrum of the selected $\eta\pi^\circ\pi^\circ$ events.

selection which is very efficient for higher $M(\eta\pi^\circ\pi^\circ)$. The selection criteria have been:

- 6 energy depositions
- neutrality
- $|\sum p_T| < 100$ MeV/c

Fig. 14 shows in the $\gamma\gamma$ invariant mass distribution the π° and the η above the combinatorial background. The next selection step is the

- event definition as $\eta\pi^\circ\pi^\circ$ by selecting that one with the smallest $\chi^2(\eta\pi^\circ\pi^\circ)$ among the 15 possible combinations.

$$\chi^2(\eta\pi^\circ\pi^\circ) = \left(\frac{M_{\gamma\gamma}^{\text{high}} - M_\eta}{\sigma(M_{\gamma\gamma})}\right)^2 + \left(\frac{M_{\gamma\gamma}^{\text{medium}} - M_{\pi^\circ}}{\sigma(M_{\gamma\gamma})}\right)^2 + \left(\frac{M_{\gamma\gamma}^{\text{low}} - M_{\pi^\circ}}{\sigma(M_{\gamma\gamma})}\right)^2$$

Similarly one calculates

- $\chi^2(\pi^\circ\pi^\circ\pi^\circ)$.

It has to be stressed that the error

$$\sigma(M_{\gamma_1\gamma_2}) = f(E_1, E_2, \theta_1, \theta_2, \phi_1, \phi_2)$$

has to be calculated correctly to get a flat probability distribution. Then one requires

- ≥ 1 configuration with $\chi^2(\eta\pi^\circ\pi^\circ) < 9$
- no configuration with $\chi^2(\eta\pi^\circ\pi^\circ) < 9$

The invariant mass spectrum of the remaining 317 events in the mass interval

$$800 \text{ MeV/c}^2 \leq M(\eta\pi^\circ\pi^\circ) \leq 2500 \text{ MeV/c}^2$$

is shown in Fig. 15. The η'–peak is the overwhelming feature (266 events). Its width equals the calculated mass resolution of 25 MeV. The $\gamma\gamma$ partial width

$$\Gamma_{\gamma\gamma}(\eta') = (4.53 \pm 0.28 \pm 0.51) \text{ keV} \quad \text{(preliminary)}$$

is found in agreement with previous measurements.

We want to study the events above the η' and ask the question: "Are they genuine $\gamma\gamma \to \eta\pi^\circ\pi^\circ$ events or are they remnants from background?" To answer this question we study the p_T^2–distribution (Fig. 16) and the $\gamma\gamma$ invariant mass distribution $M_{\gamma\gamma}$ of the remaining pair when the event contains already two π°'s (Fig. 17).

This is done for four different regions of $M(\eta\pi^\circ\pi^\circ)$, two and three of them are shown, respectively. In the η'–region one clearly sees η–mesons and the p_T^2–distributions peaks as expected for $\gamma\gamma$–reactions. On the other hand, in the $M(\eta\pi^\circ\pi^\circ)$–region from 1100 MeV/c² to 1600 MeV/c² no η's are found and the p_T^2–distribution is flat. These events are background. But in the third region, 1600 MeV/c² $\leq$ $M(\eta\pi^\circ\pi^\circ) \leq$ 2100 MeV/c², one gets η–mesons and the p_T^2–distribution peaks. These 31 events are genuine $\gamma\gamma$–events! In the fourth mass region one cannot draw definite conclusions as there are only eight events.

Further study concentrates on the mass range around $M(\eta\pi^\circ\pi^\circ) \sim 1850$ MeV/c². Fig. 18 shows the invariant mass distributions of the $\eta\pi^\circ$– and the $\pi^\circ\pi^\circ$–subsystems. In the $\eta\pi^\circ$–subsystem one sees isobars: the fit gives 70% $a_2(1320)$ plus 30% $a_0(980)$ (with $\pm$ 20% error). The $\pi^\circ\pi^\circ$–subsystem shows no structure.

Two angular distributions can be studied (Fig. 19). The direction of the η–meson and the normal to the $\eta\pi^\circ\pi^\circ$–plane, both in the center-of-mass system, with respect to the beam direction are in better agreement with the assumption of a $J^P = 2^-$ resonance production and subsequent decay into $a_2\pi^\circ$ and $a_0\pi^\circ$ isobars (which then decay to $\eta\pi^\circ\pi^\circ$) than with the assumption of phase space production and decay. Unluckily the data sample (31 events) is too small to determine the spin-parity assignment unambiguously.

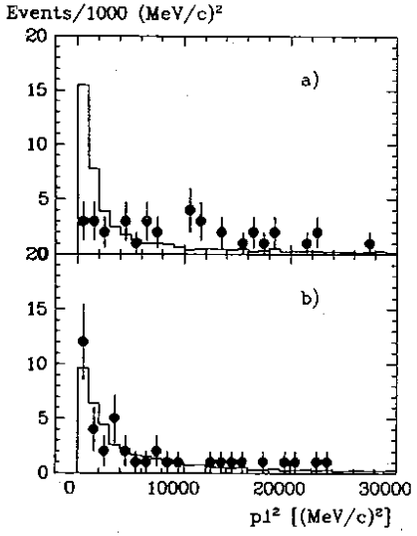

Figure 16: The p_T^2−distribution of $\eta\pi^\circ\pi^\circ$ events, a) for the $M(\eta\pi^\circ\pi^\circ)$ range from 1100 to 1600 MeV/c², b) for 1600 to 2100 MeV/c², Data: points with error bars, MC: full line.

The detection efficiency for the process

$$e^+e^- \to e^{+'}e^{-'}\gamma\gamma \to e^{+'}e^{-'}\eta\pi^\circ\pi^\circ \to e^{+'}e^{-'}(6\gamma)$$

is calculated assuming a $J^P = 2^-$ state and the $a_2\pi^\circ$ and $a_0\pi^\circ$ isobars. It depends strongly on the assumptions. Fig. 20 shows the results.

Now the Monte Carlo prediction can be fitted to the event spectrum. Fig. 21 shows the data together with the fit split into a Breit-Wigner resonance and the background ($\sim$ 10%). A resonance, called $X(1900)$, around $M(\eta\pi^\circ\pi^\circ) = 1900$ MeV/c² is seen. The resonance parameters are

$$M(X) = (1876 \pm 35 \pm 45)\ \text{MeV/c}^2$$

$$\Gamma_{tot}(X) = (228 \pm 90 \pm 34)\ \text{MeV/c}^2$$

$$\Gamma_{\gamma\gamma}(X)\,BR(X \to \eta\pi^\circ\pi^\circ) = (0.9 \pm 0.3 \pm 0.5)\ \text{keV}$$

The main sources of the systematic error are

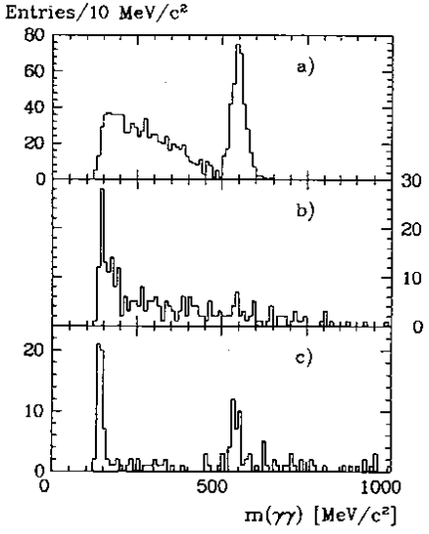

Figure 17: The $\gamma\gamma$ invariant mass for events where two π°'s have been identified, a) for the η' mass region $M(\eta\pi^\circ\pi^\circ)$ from 850 to 1100 MeV/c², b) for 1100 to 1600 MeV/c², c) for 1600 to 2100 MeV/c².

for M: energy calibration

for Γ_{tot}: background subtraction, model dependence

for $\Gamma_{\gamma\gamma}\,BR$: model dependence (33%), background (12%), efficiency (8%), luminosity (3%)

We can now try to answer the question: what is the resonance which has been observed in $X(1900) \to \eta\pi^\circ\pi^\circ$?

- We know
  - $C = +1$ from formation in $\gamma\gamma$−reactions,
  - $J \neq 1$ from formation and quasi-real $\gamma\gamma$−reactions,
  - $I = 0, 2$ from $\eta\pi^\circ\pi^\circ$ decay channel.
- We assume that it is <u>one</u> resonance, the data show no indication of a double peak.

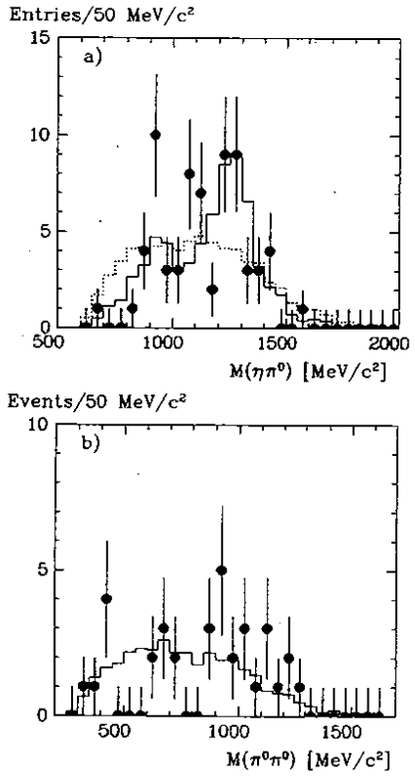

Figure 18: The invariant mass distributions of a) the $\eta\pi^\circ$− and b) the $\pi^\circ\pi^\circ$−subsystems of $\eta\pi^\circ\pi^\circ$. Data: points with error bars, MC with $J^{PC} = 2^-$ and $a_2\pi^\circ$ and $a_0\pi^\circ$ isobars: fall line, MC with phase space: dashed line.

- $J^P = 2^-$ is favoured by the angular distributions.
- The decay isobars $a_2\pi^\circ$ and $a_0\pi^\circ$ have been observed.
- Guesses on the branching ratios can be made by taking into account that $BR(a_2 \to \eta\pi^\circ) = 14.5\%$ and $BR(a_0 \to \eta\pi^\circ) = 70\%$. Using the measured

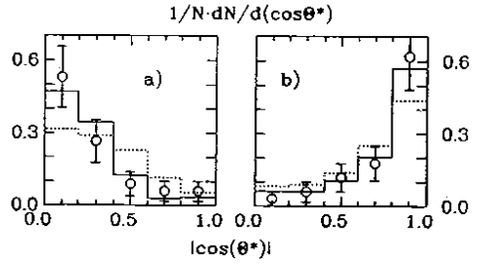

Figure 19: Angular distributions of the $\eta\pi^\circ\pi^\circ$ final state (in the $\gamma\gamma$ center-of-mass system). a) The η−direction w.r.t. the beam. b) The normal to the decay plane w.r.t. the beam. Explanations in Fig. 18

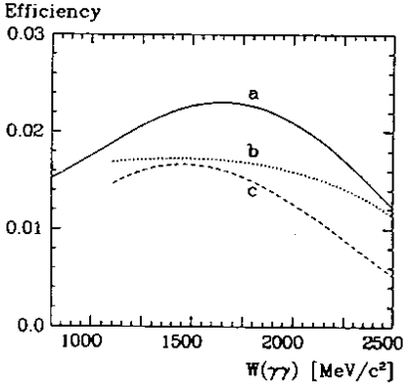

Figure 20: The detection efficiency for $\gamma\gamma \to \eta\pi^\circ\pi^\circ \to 6\gamma$'s for a) production with constant cross section and phase space decay (full line), b) $J^P = 2^-$ resonance production with decay via $a_2\pi^\circ$ isobar (dotted line), c) $J^P = 2^-$ resonance production with decay via $a_0\pi^\circ$ isobar (dashed line).

branching ratios

$$BR\left(X \to \left\{ \begin{matrix} a_2\pi^\circ \\ a_0\pi^\circ \end{matrix} \right\} \to \eta\pi^\circ\pi^\circ\right) = \left\{ \begin{matrix} (70 \pm 20) \\ (30 \pm 20) \end{matrix} \right. \quad (3.4)$$

we find

$$BR(X \to \eta\pi^\circ\pi^\circ) \leq 19\% \quad (3.5)$$

where the equal sign is valid if the $a_2\pi^\circ$ and $a_0\pi^\circ$ are the only decay modes. Using this result to-

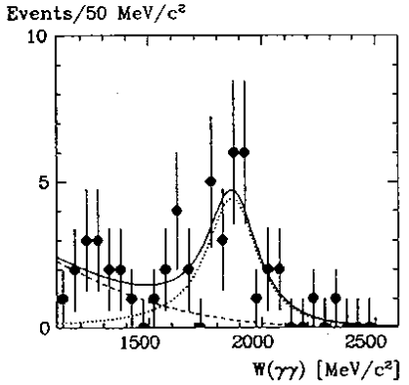

Figure 21: The fit to the $\eta\pi^\circ\pi^\circ$ mass spectrum. Breit-Wigner resonance curve: dotted line, sum: full line.

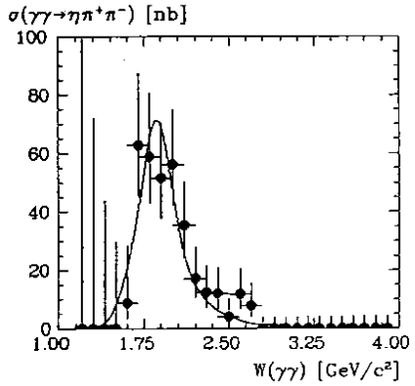

Figure 22: The cross section for $\gamma\gamma \to \eta\pi^+\pi^-$ (CELLO data). Data: points with error bars.

gether with the result on $\Gamma_{\gamma\gamma}(X)\,BR(\eta \to \pi^\circ\pi^\circ)$ we find the lower limit

$$\Gamma_{\gamma\gamma}(X(1900)) \geq 4.7 \text{ keV} \qquad (3.6)$$

where the equal sign applies if the observed decay isobars saturate all decay modes.

- The quark model predicts a $J^{PC} = 2^{-+}$ nonet ($^1D_2$ states). Its isovector member π_2 has been observed. For the isoscalar η_2 it is predicted
  - $M \sim 1700$ to 1800 MeV/c²
  - $\Gamma_{tot} \sim 400$ MeV
  - dominant decay mode $\eta_2 \to a_2\pi^\circ(\to \eta\pi^\circ\pi^\circ)$
  - $\Gamma_{\gamma\gamma} \sim 4$ to 5 keV
    (from $\Gamma_{\gamma\gamma}(\eta_2) = (25/9)\Gamma_{\gamma\gamma}^{meas}(\pi_2)$, i.e. assuming non-strange quark content)
- Combining our present knowledge the assignment

$$X(1900) = \eta_2$$

is favoured, though it cannot be shown unambiguously.

PS! The LASS group has shown evidence for the η_2' at 1.85 GeV/c² in a $K\bar{K}\pi$ phase shift analysis in the reaction $K^-p \to K\bar{K}\pi\Lambda^\circ$.

The CELLO group has presented data [13] for the reaction

$$\gamma\gamma \to \eta\pi^+\pi^- \quad \begin{cases} \hookrightarrow \gamma\gamma & \sim 25 \text{ events} \\ \hookrightarrow \gamma\gamma\pi^+\pi^- & \sim 15 \text{ events} \end{cases}$$

They observe also the $X(1900) = \eta_2$-peak (Fig. 22). A single resonance fit gives (preliminary)

$$M(X) = (1850 \pm 50) \text{ MeV/c}^2$$

$$\Gamma_{tot}(X) = (380 \pm 50) \text{ MeV}$$

$$(2J+1)\Gamma(X)\,BR(X \to \eta\pi^+\pi^-) = (15 \pm 5) \text{ keV}$$

4. SUMMARY OF CRYSTAL BALL RESULTS

For a consistent presentation of the measured $\gamma\gamma$ partial width of resonances, $\Gamma_{\gamma\gamma}(R)$, and of upper limits of states searched-for the helicity coupling constants (form factors) are very well suited [11]. The phase space is factorized out and it is proportional to the matrix element. Instead of giving the derivation I will just compile the relation between $\Gamma_{\gamma\gamma}$ and F_λ (λ = helicity of the $\gamma\gamma$ initial state) for various J^P:

0^-	$\Gamma_{\gamma\gamma} = (1/64\pi)\,M_R^3 F_0^2$
$2^+,\ \lambda = 2$	$\Gamma_{\gamma\gamma} = (1/80\pi)(1/M_R)\,F_2^2$
$2^+,\ \lambda = 0$	$\Gamma_{\gamma\gamma} = (1/240\pi)\,M_R^3\,F_0^2$
0^+	$\Gamma_{\gamma\gamma} = (1/16\pi)(1/M_R)\,F_0^2$
$2^-,\ \lambda = 0$	$\Gamma_{\gamma\gamma} = (1/120\pi)\,M_R^3\,F_0^2$

Fig. 23 shows the results on F_λ for tensor (2^{++}) and scalar (0^{++}) mesons, Fig. 24 those for pseudoscalar (0^{-+}) and 2^{-+} mesons. Given are the values for the observed resonances. Upper limits for other states, expected like radially excited mesons and glueballs or purely hypothetical, can be measured only as $\Gamma_{\gamma\gamma}(R)\,BR(R \to \text{f.s.})$. So assumptions on the branching ratio have to be made. Similarly an assumption on the total width of those resonances has to be made.

The results can be summarized by

$$F_0(\pi^\circ) \approx F_0(\eta) \approx 0.75 \times F(\eta') \approx 3.7 \times (\eta_c)$$

$$F_2(a_2) : F_2(f_2) \approx \langle e_q^2 \rangle_{a_2} : \langle e_q^2 \rangle_{f_2},$$

i.e. the wave function overlap integrals for a_2 and f_2 are equal. From these data the singlet-octet mixing angle will be derived (chapter 5). No other resonance has been seen. Limits for candidates for radially excited pseudoscalars are:

$$F_0(\pi(1300)) \leq 0.3 \times F_0(\pi^\circ) \text{ assuming}$$
$$BR(\pi(1300) \to 3\pi^\circ) = 30\%$$

$$F_0(\eta(1275)) \leq 0.3 \times F_0(\eta) \text{ assuming}$$
$$BR(\eta(1270) \to \eta\pi^\circ\pi^\circ) = 30\%$$

Similar values are obtained for other radially excited pseudoscalars in the mass range up to 2000 MeV/c².

Among the scalar mesons only the $a_0(980)$ is observed unambiguously. Its isoscalar partner $f_0(975)$ is reported as a two to three standard deviation effect by two collaborations. The values of their helicity coupling constants F_0 are an order of magnitude smaller than those for the tensor mesons. This gave rise to speculations for an exotic nature of the $a_0(980)$ and the $f_0(975)$. The $f_0(1400)$, hidden under the dominant $f_2(1270)$, should show up in the angular distribution

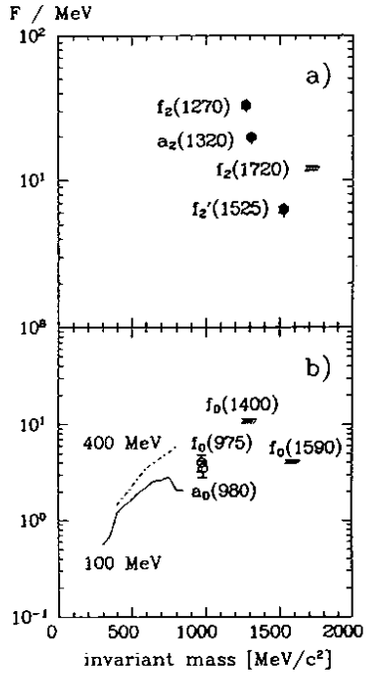

Figure 23: The helicity coupling constant F for a) tensor mesons, b) scalar mesons. Besides measured values (circles with error bars) also upper limits for glueball candidates and hypothetical resonances are given (lines with hatches). The limits for hypothetical resonances depend on the assumption of their total width, two examples are given.

of the $\pi\pi$ final state. No sign of it was found, so we get an upper limit. But it has to be mentioned that an analysis of all available $\pi\pi$–data shows evidence for the $f_0(1400)$ [17].

The matrix element of the 2^{-+} mesons π_2 and η_2 depends on the second derivative of the wave function, ψ'', because of the $L = 2$ angular momentum. Their helicity coupling constants are about the same as for the pseudoscalar mesons

$$F(\pi_2) = 0.4 \times F(\pi^\circ)$$

$$F(\eta_2) = 1.6 \times F(\pi_2)$$

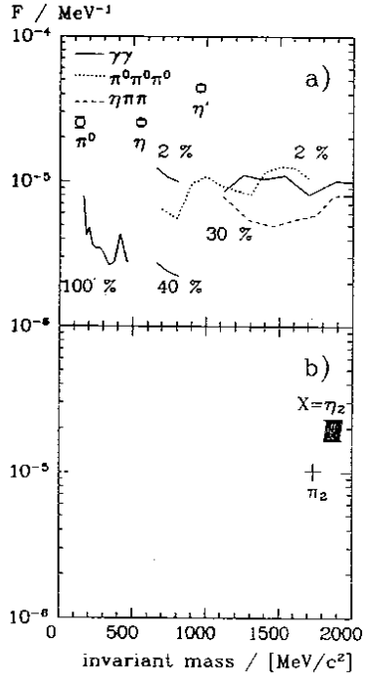

Figure 24: The helicity coupling constant F for a) pseudoscalar $J^{PC} = 0^{-+}$ mesons, b) $J^{PC} = 2^{-+}$ mesons. Besides measured values (circles with error bars, a band for $X = \eta_2$) upper limits on hypothetical resonances are given. Those values depend on the assumption for the branching ratio of the resonance into the final state.

One may therefore assume they are $q\bar{q}-$mesons.

None of the glueball candidates has been observed in $\gamma\gamma-$formation. The limits are

$$F_0(\eta(1440) = \iota) \leq 0.15 \times F_0(\pi^\circ)$$

$F_2(f_2(1720) = \Theta) \leq 0.63 \times F_2(a_2)$ assuming $BR(\Theta \to \eta\eta) = 18\%$, i.e. assuming that the main decay modes are known.

$F_0(f_0(1590)) \leq F_0(a_0(980))$ assuming $BR(a_0 \to \eta\pi^\circ) = 80\%$, $BR(f_0(1590) \to \eta\eta) = 27\%$ from the known decays.

In summary one can say that the $\gamma\gamma-$coupling of many mesons is known experimentally and we will see in the following chapter which conclusions on the meson constituents can be drawn. On the other hand the limits for glueball candidates should still be improved.

5. INTERPRETATION OF THE DATA

5.1. Singlet-octet mixing

The $SU(3)$ symmetry mixes the $u\bar{u}$, $d\bar{d}$, and $s\bar{s}$ quark content of isoscalar mesons into an $SU(3)-$octet and an $SU(3)-$singlet. Because of the heavier mass of the $s-$quark $SU(3)$ is broken and one has singlet-octet mixing. One speaks of "ideal mixing" if one of the isoscalar mesons is pure $s\bar{s}$. This corresponds to a singlet-octet mixing angle of 35.3°. From $\gamma\gamma-$reactions results on the singlet-octet mixing are available for the 2^{++} and 0^{-+} nonets. The results are

- The 2^{++} tensor meson nonet is nearly ideally mixed ($\Theta_T = (30.8 \pm 1.8)^\circ$).
- The 0^{-+} pseudoscalar meson nonet is not ideally mixed ($\Theta_P = -(21.2 \pm 1.6)^\circ$).

Next we want to see which conclusions we can draw from the existing measurements on the π_2- and η_2-mesons (assuming $X(1900) = \eta_2$). From the measurements reported here we get for the ratio of the helicity coupling constants

$$\frac{F_0^2(\eta_2)}{F_0^2(\pi_2)} \geq 2.6 \pm 1.2 \qquad (5.1)$$

This limits $F_0^2(\eta_2')$ of the second isoscalar 2^{-+} as is shown in Fig. 25. The helicity coupling constants of the two isoscalar mesons of a nonet are related. Though we have for η_2 only a lower limit with a large error one can see from Fig. 25 that $F(\eta_2')$ will be small though the mixing angle is undetermined.

A warning should be added. A calculation in a non-relativistic quark model [18] gives

$$F^{\text{model}}(2^{-+} \text{ mesons}) \leq 1/10 \times F^{\text{exp}}(\pi_2)$$

while the model predictions for the tensor mesons ($J^P = 2^{++}$) agree with the measurements.

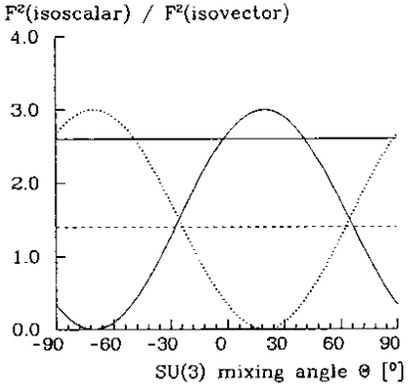

Figure 25: The ratio of the squared helicity coupling constants for the isoscalar and the isovector members of the $J^{PC} = 2^{-+}$ nonet. The $F-$values for the two isoscalars are correlated (η_2: full curve, η_2': points). The measured value for η_2 and π_2, a lower limit, is represented by the full horizontal line for the central value, and by the broken line including the errors.

5.2. Comparison of $\gamma\gamma \to R$ with $gg \to R$

As mentioned already in the introduction the coupling $gg \to R$ can be obtained from radiative $J/\psi-$decays $J/\psi \to \gamma gg \to \gamma R$. As a quantitative measure for the relative coupling strength of a resonance R to gluons and to photons, respectively, we use the stickiness S [19]

$$S = \frac{\text{coupling } R \to gg}{\text{coupling } R \to \gamma\gamma} = \frac{\Gamma(J/\psi \to \gamma R)/k_\gamma^3}{\Gamma(R \to \gamma\gamma)/m_R^3} \qquad (5.2)$$

where the partial widths are corrected for phase space (here for 0^--mesons). Normally one uses the stickiness relative to that of the $\eta-$meson:

$$S_{\text{rel}}(R) = S(R)/S(\eta) \qquad (5.3)$$

The data for $J/\psi \to \gamma\eta\pi\pi$ are scarce, for $J/\psi \to \gamma\pi\pi\pi$ non-existing. The Crystal Ball measurements [20] of $J/\psi \to \gamma\eta\pi^+\pi^-$ and $\to \gamma\eta\pi^\circ\pi^\circ$ has been described by a broad resonance with

$$M = (1770 \pm 45) \text{ MeV/c}^2$$

$$\Gamma_{tot} = (520 \pm 110) \text{ MeV}$$

$$BR(J/\psi \to \gamma(\eta\pi\pi)_{1770}) = (6.5 \pm 0.3 \pm 0.8) \times 10^{-3}$$

A spin parity analysis has not been made.
Mark III results [21] are in qualitative agreement, but a quantitative analysis is presented till now only for $M < 1500$ MeV/c².

If we want to calculate $S_{\text{rel}}(\eta_2)$ we have to make some assumptions:
resonance X seen in $\gamma\gamma \to \eta\pi\pi$ is η_2,
resonance X seen in $J/\psi \to \gamma\eta\pi\pi$ is η_2.
Then we find

$$S_{\text{rel}}(\eta_2) = 0.42. \qquad (5.4)$$

What happens if these assumptions are only partially true, i.e. if in the radiative $J/\psi-$decay more states are produced than the η_2? The stickiness will decrease. But a wrong interpretation can only come from an overestimation of S_{rel}.

Before drawing the conclusion let me remind you of the results on $S_{\text{rel}}(\equiv S)$:

$$J^{PC} = 0^{-+} : S(\pi^\circ) : S(\eta) : S(\eta') : S(\iota)$$
$$= 3.3 \times 10^{-2} : \mathbf{1} : 3.1 : (> 49)$$

Comparing this existing knowledge with the result of eq.(5.4) we can conclude that the η_2 seems to be a $q\bar{q}-$meson.

6. SUMMARY

The Crystal Ball detector has been used to measure resonance formation in $\gamma\gamma-$reactions. A wide range of final states has been observed and resonances have been identified:

$\gamma\gamma$	$\to \gamma\gamma$:	π°, η, η'
	$\to \pi^\circ\pi^\circ$:	$f_2(1270)$, $f_0(975)$
		threshold continuum
	$\to \pi^\circ\eta$:	$a_0(980)$, $a_2(1320)$
		threshold continuum
	$\to \pi^\circ\pi^\circ\pi^\circ$:	η, $\pi_2(1670)$
	$\to \eta\pi^\circ\pi^\circ$:	η', $X(1900)(= \eta_2?)$

Besides the two-photon partial width $\Gamma_{\gamma\gamma}$ of the observed resonances limits on other states, especially on candidates for radial excitations and for glueballs, have been given.

New results are the two-photon formation of the $\pi_2(1670)$ in the $\pi^\circ\pi^\circ\pi^\circ$ channel and of a hitherto unknown resonance X at $M(X) =$ MeV/c^2. The Crystal Ball obtained $\Gamma_{\gamma\gamma}(\pi_2) = (1.41 \pm 0.23 \pm 0.28)$ keV which is also the first observation of the neutral π_2^0. Because of the small event number a unique assignment of the quantum numbers of X cannot be made. The best fit to the decay isobar spectrum and the angular distributions gives $J^{PC} = 2^{-+}$ suggesting that X is the η_2, the isoscalar partner to the π_2. The size of the $\Gamma_{\gamma\gamma}$'s lets us suppose that the 2^{-+} mesons are $q\bar{q}$ states.

The existing data on the two-photon partial width of meson resonances are presented by their helicity coupling constants F_λ ($\lambda =$ helicity). Here phase space is factorized out and the quantity is proportional to the matrix element of the process. This gives easily an intuitive understanding of the result. So the $\Gamma_{\gamma\gamma}$ for the η' and the π° are a factor of ~ 600 different, but the helicity coupling constant of the η' is only a factor of ~ 2 larger than that of the π°, indicating on the first glance that their constituents are not qualitatively different. Theory has to explain this factor of 2.

The physics analysis starts from the fact that photons couple to charges. So the $\gamma\gamma-$coupling probes the charge constituents (quarks and gluons) of resonances. Comparing the resonances within a nonet one can learn about non-strange and strange quark content of the isoscalar resonances (singlet-octet mixing). While in the $J^{PC} = 2^{++}$ tensor meson nonet the non-strange and strange quarks decouple, they are mixed for the $J^{PC} = 0^{-+}$ pseudoscalar mesons. Information on possible gluon constituents of a resonance can be obtained by comparing $\gamma\gamma \to R$ with $gg \to R$ which is extracted from radiative $J/\psi \to \gamma R$ decays. This is expressed by the quantity "stickiness". The best gluonium candidates (ι/η (1440) and θ/f_2 (1770)) are not observed in $\gamma\gamma-$formation. So $\gamma\gamma-$reactions contribute to "hadron microscopy".

REFERENCES

1. D. Antreasyan et al., Phys. Rev. D 33(1986)1847.
2. D. Antreasyan et al., Phys. Rev. D 36(1987)2633.
3. D.A. Williams et al., Phys. Rev. D 38(1988)1365.
4. H. Marsiske et al., Phys. Rev. D 41(1990)3324.
5. D. Antreasyan et al., DESY 90-054, Z. Phys. C, in print.
6. K. Karch et al., DESY 90-068, Phys. Lett. B, in print.
7. D. Sievers, Ph.D. thesis, Univ. Hamburg (1989), Internal report DESY-F31-89-04.
8. R.N. Cahn, in: "Procs. 1989 Symposium on Lepton and Photon Interactions at High Energies", Stanford, CA, (World Scientific; Singapur 1990), p. 60.
9. S. Cooper, Ann. Rev. Nucl. Part. Sci. 38(1988)705.
10. H. Kolanoski and P. Zerwas, in: "High Energy Electron-Positron Physics", A. Ali and P. Soeding (Eds.), (World Scientific, Singapur 1988), p. 635.
11. M. Poppe, Int. J. Mod. Phys. A1(1986)545.
12. H.-J. Behrend et al., Z. Phys. C 46(1990)583.
13. H.J. Behrend et al., Contributed paper to 25th International Conference on High Energy Physics, Singapur, 1990.
14. E.D Bloom and C. Peck, Ann. Rev. Nucl. Part. Sci. 33(1983)143.
15. K. Wachs et al., Z. Phys. C 42(1989)33.
16. J.J. Hernández et al., Particle Data Group, Phys. Lett. B239(1990)1.
17. D. Morgan and M.R. Pennington, preprint RAL-90-030(1990).
18. J.D. Anderson et al., preprint LBL-29059(1990).
19. M.S. Chanowitz, in: 6th Int. Workshop on Photon-Photon Collisions, Granlibakken, Lake Tahoe, Sept. 1984 (World Scientific, 1985).
20. C. Edwards et al., Phys. Rev. Lett. 51(1983)859.
21. J.J. Becker, Ph.D. Thesis, University of Illinois, Urbana-Champaign (1984).